Reconstructing influenza incidence by deconvolution of daily mortality time series

Edward Goldstein[a,1], Jonathan Dushoff[b,c], Junling Ma[d], Joshua B. Plotkin[e], David J. D. Earn[c,d], and Marc Lipsitch[a]

[a]Center for Communicable Disease Dynamics, Department of Epidemiology, Harvard School of Public Health, Boston, MA 02115; [b]Department of Biology, McMaster University, Hamilton, ON, Canada L8S 4K1; [c]M. G. Degroote Institute for Infectious Disease Research, McMaster University, Hamilton, ON, Canada L8N 3Z5; [d]Department of Mathematics and Statistics, McMaster University, Hamilton, ON, Canada L8S 4K1; and [e]Department of Biology, University of Pennsylvania, Philadelphia, PA 19104

Edited by Burton H. Singer, Princeton University, Princeton, NJ, and approved October 23, 2009 (received for review March 17, 2009)

We propose a mathematically straightforward method to infer the incidence curve of an epidemic from a recorded daily death curve and time-to-death distribution; the method is based on the Richardson–Lucy deconvolution scheme from optics. We apply the method to reconstruct the incidence curves for the 1918 influenza epidemic in Philadelphia and New York State. The incidence curves are then used to estimate epidemiological quantities, such as daily reproductive numbers and infectivity ratios. We found that during a brief period before the official control measures were implemented in Philadelphia, the drop in the daily number of new infections due to an average infector was much larger than expected from the depletion of susceptibles during that period; this finding was subjected to extensive sensitivity analysis. Combining this with recorded evidence about public behavior, we conclude that public awareness and change in behavior is likely to have had a major role in the slowdown of the epidemic even in a city whose response to the 1918 influenza epidemic is considered to have been among the worst in the U.S.

1918 pandemic | incidence curve | death curve | Richardson–Lucy deconvolution | infectivity ratios

In characterizing a newly emerging or historical epidemic, one often has access to an epidemic curve that provides the number of persons who became ill on a certain day (the symptom curve), or the number of cases that were reported each day (the report curve), or the number of dying that were reported each day (the death curve). Of more direct interest, for the purposes of visualizing the spread of the epidemic and calculating relevant quantities such as the daily reproductive number, is the (usually unobserved) epidemic curve of the number of persons becoming infected on each day (the incidence curve). The other three curves—the symptom, report, and death curves—provide information about the incidence curve but are imperfect representations of it, first because not all cases may appear in these other curves—asymptomatics, unreported cases, or nonfatal cases respectively will be missed—and perhaps more importantly because the delay between infection and subsequent events—symptom onset, report, or death—is a random variable that adds horizontal variation or "smear" to the epidemic curve. For some infections (e.g., HIV), diagnostic symptoms (i.e., AIDS-defining illness) may occur years after infection, so the symptom curve is a poor reflection of the evolution of the epidemic; there is much literature on the problem of deconvolution to estimate the HIV incidence curve from the symptom (AIDS-incidence) curve (1). For acute infections, such as SARS and influenza, the incubation period is relatively short compared with the growth rate of the epidemic; hence the symptom curve and the incidence curve are similar. The time to death for such infections, however, can be several weeks, equivalent to three or more disease generations, and is highly variable (2–4), making the death curve a poor surrogate for the incidence curve.

In this paper, we propose a mathematically straightforward method to infer the incidence curve from a death curve. The incidence curve is then used to estimate the basic epidemiological quantities of interest, such as the daily reproductive numbers and infectivity ratios; the latter can be utilized to assess major changes in the epidemic's dynamics.

First, we describe a technique for deconvolution to estimate the incidence curve from the death curve and the time-to-death distribution. The technique, called the Richardson-Lucy (RL) deconvolution, was originally developed for use in optics (5, 6), and is adapted in a simple way to the slightly different setting of the death-to-incidence deconvolution problem. The technique is illustrated for the 1918 influenza epidemic in Philadelphia and New York State (2, 7, 8).

Second, we use the reconstructed incidence curves to perform inference on daily reproductive numbers in that epidemic. One level of difficulty arises from the fact that because of the rapid progression of the epidemic, there is saturation of susceptibles and a possible change in behavior during the course of infection for persons infected on a given day (9). To deal with this issue, we have rederived the Wallinga–Teunis estimator by using an approach similar to the one in ref. 10. The derivation uses daily infectivity ratios, a concept which essentially appeared before in refs. 10 and 11.

Third, we examine the spread of pandemic influenza in the city of Philadelphia around the end of September and the beginning of October, 1918. On September 28, a 200,000-person Liberty Loan Drive took place on the streets of Philadelphia against the advice of medical professionals (12). Within 72 hours, "every single bed in the city's 31 hospitals was filled" (ref. 13, p. 220). By October 1, residents were often encouraged to stay home to stem spread of the disease (14). On the evening of October 3, the closure of schools, churches, and places of public amusement was adopted by the Philadelphia city council (ref. 15, p. 74). The deconvolved incidence curve, which peaks around October 1–2, shows a drastic change in the growth patterns/infectivity ratios between September 26 and October 3. In particular, the infectivity ratios, representing the average number of infections by an infector on a given day, dropped by more than half. We estimate, assuming that case-fatality ratio is at least 2% (16, 17), that during this period depletion of susceptibles was at most 16% (here and elsewhere, depletion is characterized in terms of the number of susceptibles on September 26, which equals Philadelphia's population minus the number of infected by September 25). This difference suggests that depletion of susceptibles played only a modest role in slowing the growth of the epidemic during that period, which took place before the closures went into effect. Our main conclusion, which is not merely of historical interest, is that public awareness

Author contributions: E.G., J.D., J.M., J.B.P., D.J.D.E., and M.L. designed research; E.G., J.D., J.M., J.B.P., D.J.D.E., and M.L. performed research; E.G., J.D., J.M., J.B.P., D.J.D.E., and M.L. analyzed data; and E.G. and M.L. wrote the paper.

The authors declare no conflict of interest.

This article is a PNAS Direct Submission.

Freely available online through the PNAS open access option.

[1]To whom correspondence should be addressed. E-mail: egoldste@hsph.harvard.edu.

This article contains supporting information online at www.pnas.org/cgi/content/full/0902958106/DCSupplemental.

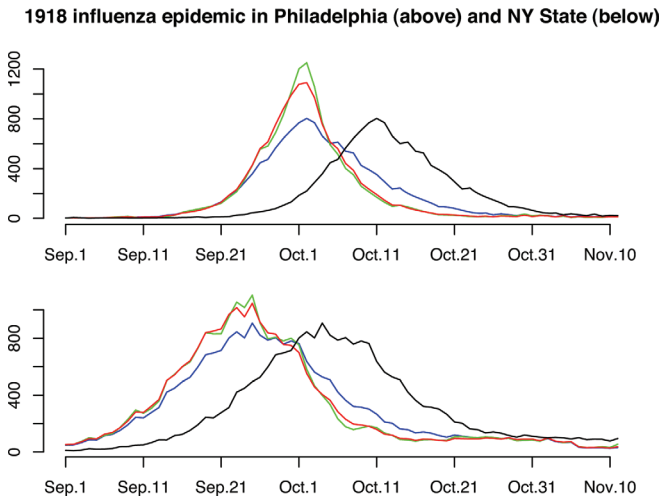

Fig. 1. The influenza epidemic in Philadelphia (*Upper*) and New York State (*Lower*) in 1918. Black is death curve. Blue is the initial condition for RL iterations (death curve, shifted back by nine days). Red is the estimated incidence (scaled by a factor of p, where p is the case fatality ratio), obtained from the first iteration for which the χ^2 value from Eq. **3** is below 1 (sixth iteration for Philadelphia and fourth iteration for New York State). Green are results of RL after 30 iterations.

and changes in behavior are likely to have had a major role in the slowdown of the epidemic before the official control measures were in place.

In the *SI Appendix* we use simulations and sensitivity analyses to test the robustness of our methodology/conclusions. We examine how well the deconvolved incidence curve represents the original one, and what is the best way to estimate the growth rate and the initial reproductive number of the original incidence curve. We also study the epidemic progression in Philadelphia between September 26 and October 3, considering various "incidence" curves deconvolved by using a collection of randomly generated time-to-death distributions and also allowing for time dependency of the case-fatality ratios due to potential changes in demographics of the infected. Our general conclusion remains valid in all cases: Within that period, a drastic change in the epidemic's dynamics took place, and depletion of susceptibles was probably insufficient to explain that development.

Results

Reconstructing the Daily Incidence Curves for the 1918 Influenza Epidemic. We apply the procedure from the *Methods* section to the 1918 influenza and pneumonia death curves in Philadelphia and New York State (excluding the city) to obtain the daily incidence in those places. Fig. 1 depicts the reconstructed incidence curves, which are scaled by a factor of p, where p is the case fatality ratio. Notably, the peaks of the incidence curves are shifted backward by approximately nine days, but the incidence curves have narrower peaks with steeper upward and downward trajectories as one would expect when removing the smear induced by the time-to-death distribution, which is analogous to removing the blur due to camera motion from a photographic image.

Estimates of the Daily Reproductive Numbers. The effective reproductive number R_t on day t measures the mean number of infections caused by persons who become infected on day t. Fig. 2 plots the estimated reproductive numbers for certain periods of the epidemic's progression, in both Philadelphia and New York State. The reproductive numbers fluctuate initially because of the small values for the deconvolved incidence. The reproductive numbers descend in the later part of the exponential growth period, representing future infections which happen under saturation of susceptibles or behavior change.

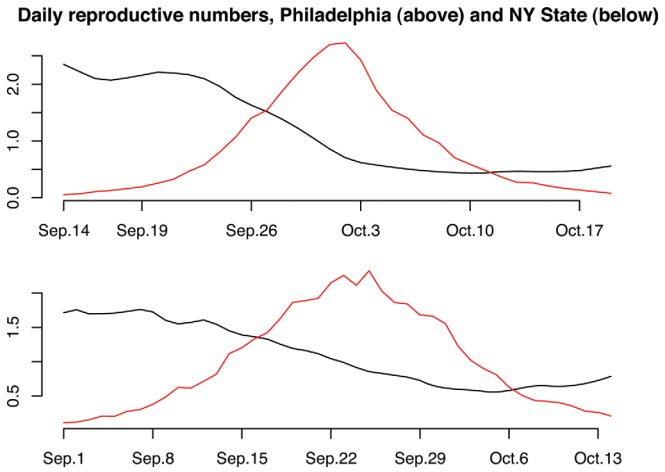

Fig. 2. Epidemic progression in Philadelphia (*Upper*) and New York State (*Lower*), for certain time periods. Red is deconvolved incidence (scaled), and black represents the estimated reproductive numbers.

With the fluctuation of the reproductive numbers, one may wonder what is the best way to estimate R_0, the mean number of new infections caused by an infected individual during the early, exponential growth stage of the actual epidemic curve in Philadelphia. We address this via simulations in the *SI Appendix*. Our estimate is $R_0 = 2.14$, with a standard error of 0.13.

Epidemic Peak in Philadelphia. In this section, we examine the peak of the Philadelphia epidemic in more detail. We first compute the daily infectivity ratios, representing the number of infections on a given day caused by a weighted average of previously infected individuals (Eq. **4**). Fig. 3 plots the estimated infectivity ratios for the period of September 14–October 19.

The infectivity ratio IR_t on a given day t presents a basic assessment of the epidemic's state on day t; in a mass action model, the infectivity ratio is proportional to the number of susceptibles left on that day. The reproductive number R_t on day t measures the number of infections caused during an infectious period of an average person who was infected on day t; it may be harder to relate R_t to the epidemic's state on day t because during that infectious period further depletion of susceptibles may occur, and conditions related to the epidemic's progression, such as an introduction of control measures and an increase in public awareness, may take place.

The estimated infectivity ratios dropped by more than half between September 26 and October 3. At the same time, depletion of susceptibles was much smaller. Philadelphia had a population of 1.7 million, with another 300,000 added by the war industry (15). As explained in Methods, the estimated incidence curve plotted in Figure 1 is scaled by a factor of p, where p is the case fatality ratio. Various estimates of p, according to location, age, gender and

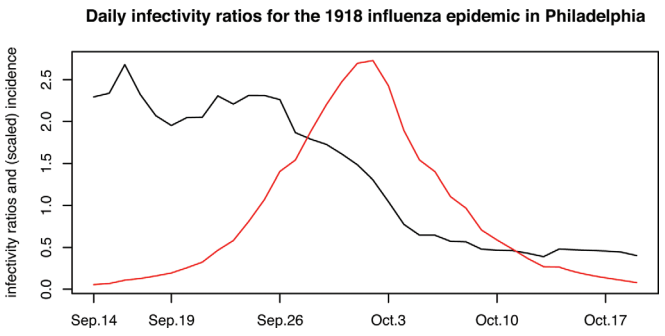

Fig. 3. Estimated infectivity ratios (black) vs. (scaled) incidence (red) in Philadelphia, September 14–October 19, 1918.

race, are given in refs. 16 and 17. There is considerable geographic variation in case-fatality ratios, and for the surveyed communities in the Northeastern United States (from Baltimore, MD to New London, CT) case-fatality ratios were above 2%, topping 3% in some places. Assuming $P \geq 0.02$ for Philadelphia and by using the deconvolved incidence curve, we estimate that at most 16% of the susceptible population was depleted between September 26 and October 3, which cannot account for the over 50% drop in the infectivity ratios during that period; the latter finding was subjected to extensive sensitivity analysis with regard to the time-to-death distribution and other parameters (see the *SI Appendix* for more details). At the same time, we have evidence from refs. 12 and 14 about public awareness of the epidemic prior to October 3. We conclude that public awareness and change in behavior likely played a major role in the slowdown of the epidemic in Philadelphia before the official control measures were implemented on October 4.

Discussion

We have described and demonstrated the usefulness of a RL-type deconvolution approach to reconstruct incidence curves from epidemic curves showing the times of death in an epidemic. Applied to the 1918 influenza data, this approach reconstructs an epidemic curve that is more sharply peaked than the death curve—as one would expect given the smear introduced by the large variance in the time-to-death distribution. Moreover, this reconstructed curve allows the direct estimation of a daily value for the reproductive number R_t, bypassing the more-cumbersome methods used previously, which involved extensive simulations and allowed the estimation of only a single value for R (4), or a parametric estimation of R_t (18). The estimate of R_t is given by the Wallinga–Teunis formula (9). Our derivation of this estimate relies on the fact that the number of infected individuals is large hence the notion of an average-infectiousness profile makes sense; this is different from the original setting of an emerging epidemic in ref. 9, where it is assumed that all infected individuals had the same infectiousness profile. Finally, the deconvolved incidence curve was used to show that public awareness and change in behavior is likely to have played a major role in the slowdown of the epidemic even in Philadelphia, a city whose response to the 1918 influenza epidemic is considered to have been among the worst in the U.S. (13, 19). A related point regarding the belatedness of official control measures in Philadelphia was made in ref. 18.

The latter qualitative conclusion was subjected to extensive sensitivity analysis. The population of Philadelphia was not homogeneous, with case-fatality ratios, time-to-death distributions, infectivity and susceptibility to infection varying by age and even gender. Although we cannot recover the complexity of the population network in Philadelphia, we have tested our observation that the drop in infectivity ratios during the week between September 26 and October 3 greatly exceeded the depletion of susceptibles under various scenarios; we have examined the sensitivity of that conclusion with respect to the time-to-death distribution, and allowed for certain forms of time dependency for the case-fatality ratios, reflecting upon potential changes in the demographics of the infected as the epidemic progressed. The main conclusion persisted with remarkable stability in the simulations we have performed. Furthermore, visual inspection of the growth rate of the death curve (Fig. 4) shows a major change in its slope by October 5–6, which was likely predated by major changes in incidence patterns. Combining this with contemporary journalistic evidence (14) suggests that our hypothesis about the change in behavior before the official control measures were implemented is likely to be real.

We have not considered asymptomatic infections in our analysis. Data from the 1957 and the 1968 influenza epidemics yielded estimates of 20–42% for the rate of asymptomatic infections (20, 21). A review of several volunteer challenge studies (22) gives an estimate of 33% for the rate of asymptomatic infections. There is no data for the rate of asymptomatic infections for the 1918 influenza pandemic. Given its virulence, that rate could have been lower than the rates above. In our simulations, the drop in infectivity ratios between September 26 and October 3 surpasses depletion of susceptibles by a factor of at least 2.5. Thus, even if a third of all infections were asymptomatic, depletion of susceptibles during that period cannot explain the drop in infectivity ratios.

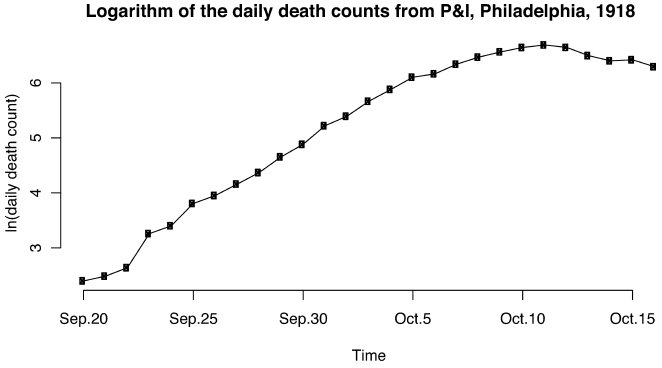

Fig. 4. Natural logarithm of the recorded daily number of deaths from pneumonia and influenza in Philadelphia, 1918.

Our approach in principle gives a general method for reconstructing an incidence curve from the death curve. In practice, to have reliable estimates one needs the standard errors of the counts to be small as compared with the means—say, if the (Poisson) counts reach into the hundreds. We recommend performing simulations following the protocol in the *SI Appendix* to see how well the deconvolution process works.

We note that estimated infectivity ratios in Philadelphia (Fig. 3) first drop on September 27, one day before the notorious Liberty Loan parade, and seven days before the implementation of official control measures. Although reductions in transmission in the absence of official control measures have been inferred from the dynamics of influenza in U.S. cities by a previous study (18), this finding for Philadelphia is surprising, given that the parade is often interpreted as a sign that Philadelphia residents had not yet recognized the seriousness of the pandemic, and, moreover, that the parade is often seen as an opportunity for large-scale transmission. If we have accurately estimated the timing of the decline in infectivity ratios, then the parade was probably not in fact a major venue for transmission, perhaps because it took place in the open air, and we must infer that behavior changes made a contribution to the slowing of the epidemic prior to official control measures. We have considered the possibility that the timing is estimated incorrectly. For example, it is possible that the time-to-death distribution we have employed is too long, resulting in artificially early changes in the incidence curve to reflect changes in the death curve. We believe that a shorter time-to-death distribution is unlikely because we are unaware of any reliable data suggesting that the time-to-death distribution is substantially shorter than the one we have adopted from ref. 2; in fact, the distribution we used is shorter than the one obtained from military data and used previously in refs. 4 and 18 (see *SI Appendix*). A likely source of error in estimating the exact timing of declines in infectivity ratios might be the nature of the deconvolution process, as seen in simulations in the *SI Appendix*. Briefly, deconvolved incidence curves have an exponential growth period ending about two days before the original one.

One may wonder if it is possible to use the death curve directly to infer epidemiological parameters of interest, such as R_0. One can try the exponential growth rate approach (see the *SI Appendix*). In theory, given a long exponential growth period for incidence (long in comparison to the time-to-death distribution), the death curve would have the same exponential growth rate. However for the Philadelphia data, deconvolution shows that the death

curve growth rate is somewhat smaller than the incidence curve growth rate, and the estimate of R_0 resulting from the death curve growth rate ($\simeq 2 - 2.02$) is biased downward. Alternatively, one can consider the Wallinga and Teunis approach for estimating the reproductive numbers by using the "death-to-death" distribution. The latter can be understood as follows: For people who died on day t, one can look at the times of death of the individuals they've infected. However this distribution depends on the state of the epidemic around time t, and thus changes with t. Moreover, assuming that the serial interval distribution is independent for different pairs of cases, the death-to-death distribution will not be independent for successive pairs of cases (e.g., A who infects B who infects C), violating the assumptions of the approach. At the same time, we found that having information about the incidence curve can be used for a number of purposes besides estimating R_0. Our estimates of the daily reproductive numbers and assessment of the rapid decline of infectivity ratios around the peak of the epidemic in Philadelphia may not be accessible directly from the death curve.

It is also worthwhile to compare the approach to estimating R_t here to an approach which assumes that future opportunities for infection for each individual, regardless of when they are infected, will follow a fixed distribution going forward in time. One might expect that the relation between the reproductive numbers, the serial interval (w_i) (see *Methods*), and new infections is that for an average person infected on day t, the expected number $E_{t,i}$ of people s/he will infect on day $t + i$ is

$$E_{t,i} = R_t \cdot w_i. \qquad [1]$$

The relation above is known to hold during periods when there is little to no depletion of susceptibles and behavior change (23)—during that period, R_t is in fact constant. However this may be untenable for the whole duration of an epidemic, where the number of susceptibles may decline over the course of a single individual's infectious period (24); similarly, measures to control the epidemic and behavior change may take place during that period. To put the issue a bit more precisely, consider the ratio $\frac{E_{t,i_1}}{E_{t,i_2}}$. If Eq. **1** was correct, this ratio would equal $\frac{w_{i1}}{w_{i2}}$ and would be independent of the day t of the infection. However, when the epidemic progresses very rapidly, populations of susceptibles (and their possible behavior) can be quite different on days $t+i_1$ and $t+i_2$. Thus, it is unreasonable to expect that this ratio is independent of t. The formulation proposed here, and in ref. 9, avoids this pitfall.

Methods

Richardson–Lucy-Type Deconvolution. The deconvolution problem is to assess the daily incidence curve (I_t) given the daily death curve ($D_1, \ldots, D_N$) and time from-infection-to-death distribution ($d_1, \ldots, d_l$). Here, D_j is the number of deaths recorded on day j; and d_k represents the probability that an infected person who will eventually die, will die on day k after his/her infection. The daily death curves for Philadelphia and New York State (excluding city) are recorded in refs. 7 and 8. The time from-infection-to-death distribution is obtained as a convolution of two distributions: time from symptom onset to death, taken from ref. 2, based on 599 hospital autopsy reports and the influenza latent period distribution, taken from ref. 25. It is plotted in Fig. 5.

To assess incidence I_t on day t, let p be the probability that an infected individual will die from influenza and pneumonia; in the *SI Appendix*, we allow for time dependence of p due to potential shifts in demographics of the infected. The number of people who got infected on day t and later died is binomial $Bin(I_t, p)$; because I_t is large and p is small, it is well approximated by a Poisson variable $Pois(\lambda_t)$ with (an unknown) mean $\lambda_t = p \cdot I_t$. Those $Pois(\lambda_t)$ deaths are binned over the subsequent days according to the time-to-death distribution.

We wish to estimate the daily incidence curve during some time period $(t_1, \ldots, t_2)$, which overlaps with the period $(1, \ldots, N)$ for which the daily counts for the number of deaths are available ($N = 92$ for Philadelphia and $N = 75$ for New York State). Because over 95% of deaths happen within three weeks of infection, we want to estimate incidence from day $t_1 = -20$ (three weeks prior to the available death data); we also take $t_2 = N - 2$ as $d_1 = 0$ for our time-to-death distribution. Thus, the number of unknown parameters is $N + 19$, exceeding the number N of observations.

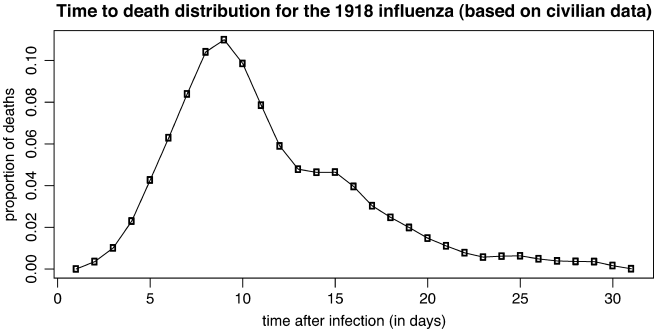

Fig. 5. Assumed proportions of deaths on each day since infection. Based on the Cook County Hospital data from ref. 2 for time from symptom onset to death and the latent period distribution from ref. 25.

To assess the vector of unknown parameters $(\lambda_{t_1}, \ldots, \lambda_{t_2})$ (thus estimating the incidence curve up to a multiple), we iterate in the space of parameters by using the expectation maximization algorithm (26); this procedure is called the RL iteration. The initial guess $\lambda^0 = (\lambda^0_{t_1}, \ldots, \lambda^0_{t_2})$ for the parameters is the death curve, shifted back by nine days, as the time-to-death distribution $(d_1, \ldots, d_{31})$ peaks on day nine after infection (see Fig. 4). RL iterations produce a sequence $\lambda^n = (\lambda^n_{t_1}, \ldots, \lambda^n_{t_2})$ of the Poisson parameters. Explicitly, let $q_j = \sum_{-j+1 \le i \le N-j} d_i$ be the probability that a death resulting from incidence on day j will be observed during the interval $1, \ldots, N$; here $-20 \le j \le N - 2$ and $d_i = 0$ for $i \le 0$ or $i \ge 32$. Let $D^n_i = \sum_{j<i} d_{i-j} \lambda^n_j$ be the expected number of deaths to occur on day i, conditional on the parameters λ^n. Then,

$$\lambda^{n+1}_j = \frac{\lambda^n_j}{q_j} \cdot \sum_{i>j} \frac{d_{i-j} D_i}{D^n_i}. \qquad [2]$$

The probability of observations $D_1, \ldots, D_N$, conditional on the Poisson parameters λ^n and the time-to-death distribution, increases with each iteration. While iterating, we do not seek convergence to a maximum likelihood solution; rather, we use a criterion to end iterations and produce our estimate of the Poisson parameters. To understand this, for the nth iteration, let $E^n_i = \sum_{j<i} \lambda^n_j d_{i-j}$ be the expected number of deaths on day i. If λ^n were the true parameters, D_i would be Poisson distributed with mean E^n_i; thus, the expectation $E(\frac{(E^n_i - D_i)^2}{E^n_i})$ would be 1. This suggests to iterate until the normalized χ^2 statistic

$$\chi^2 = \frac{1}{N} \sum_i \frac{(E^n_i - D_i)^2}{E^n_i} \qquad [3]$$

descends below 1 for the first time.

Bootsrapping simulations in the *SI Appendix* address the question of how closely a deconvolved curve resembles the original incidence curve.

Estimating Reproductive Numbers and Infectivity Ratios. In this section, we show how to estimate the daily reproductive numbers for the 1918 influenza from incidence curves and the infectiousness profile distribution. We remark that the words "infectiousness profile" and "serial interval" are often used interchangeably, though this is not quite accurate (see ref. 27, where "infectiousness profile distribution" is called "infectious contact distribution"). We prefer the term "infectiousness profile distribution" because it reflects upon average individual infectivity, which depends only on the time since one became infected, unlike the proportion of infectious contacts on each day after infection or the time between one's infection and the infection of one's infector.

We set a cutoff of 10 days for the infectivity process. The infectiousness profile distribution $(w_1, \ldots, w_{10})$, essentially taken from ref. 25, is plotted in the *SI Appendix*. Here each number w_i represents the proportion of the cumulative infectiousness which falls between days $(i - 0.5, i + 0.5)$ for an average person. Note that, conveniently, the latent period in ref. 25 has an offset of 0.5 days.

By using the infectiousness profile distribution and the incidence curve, we can describe some key epidemiological parameters of interest. The infectivity ratio IR_t on day t measures the number of people infected by an "average" infector on day t:

$$IR_t = \frac{I_t}{\sum_{i<t} I_i \cdot w_{t-i}}. \qquad [4]$$

This concept was already used in ref. 10, where it was denoted by $\phi_1(t)$, and in ref. 11, where it was denoted by R_t. If the population of susceptibles and their behavior does not change much over a reasonable interval (covering the time of one individual's infectiousness history), the infectivity ratio would equal the reproductive number. This is not the case for the epidemics in question. However, because the number of infected is large, we can compute the reproductive number R_t on day t in a "forward-looking" way, by adding up the numbers of infections caused in subsequent days by an average person who got infected on day t:

$$R_t = \sum_{i>0} \mathrm{IR}_{t+i} \cdot w_i = \sum_{i>0} \frac{w_i I_{t+i}}{\sum_{I=i-10}^{i-1} w_{i-I} I_{t+I}}. \quad [5]$$

This is the Wallinga–Teunis formula, and its derivation essentially follows ref. 11. Note that this derivation relies on the fact that the number of infected is large, hence the notion of an average infectiousness profile makes sense; this is different from the original setting of an emerging epidemic in ref. 9, where it is assumed that all the infected have the same infectiousness profile. The two derivations help to clarify the notion that the reproductive number R_t is forward-looking, taking account of all the events that may happen after time t that will affect how many secondary cases an individual infected at t will infect. By contrast, the infectivity ratio looks backward from the day on which infection occurs. In the case of exponential growth (where opportunities for transmission remain constant over time), the two measures are equivalent.

ACKNOWLEDGMENTS. M.L. and E.G. were funded by the U.S. National Institutes of Health Models of Infectious Disease Agent Study Cooperative Agreements 5U01GM076497 and 1U54GM088588 to M.L. D.J.D.E., J.M., and J.D. were supported by the Canadian Institutes of Health Research and the Natural Sciences and Engineering Research Council of Canada. D.E. and J.B.P. were supported by the J. S. McDonnell Foundation. J.B.P. was supported by the Burroughs Wellcome Fund, the David and Lucille Packard Foundation, and National Institutes of Health Grant 3U54AI057168-06S1. The authors would like to thank the Banff International Research Station for hosting focused research group meetings at which this project was begun.

1. Brookmeyer R, Gail M (1994) *AIDS Epidemiology*: *A Quantitative Approach*. (Oxford Univ Press, Oxford).
2. Brundage JF, Shanks D (2008) Deaths from bacterial pneumonia during 1918–19 influenza pandemic. *Emerging Infectious Dis* 14:1193–1199.
3. Donnelly CA, et al. (2003) Epidemiological determinants of spread of causal agent of severe acute respiratory syndrome in Hong Kong. *Lancet* 361:1761–1766.
4. Mills CE, Robins JM, Lipsitch M (2004) Transmissibility of 1918 pandemic influenza. *Nature* 432:904–906.
5. Richardson WH (1972) Bayesian-based iterative method of image restoration. *J Opt Soc Am* 62:55–59.
6. Lucy LB (1974) An iterative technique for the rectification of observed distributions. *Astronom J* 79:745–754.
7. Rogers SL (1920) *Special Tables of Mortality from Influenza and Pneumonia, in Indiana, Kansas, and Philadelphia, PA*. (U.S. Dept Commerce, Washington, DC).
8. Eichel OR (1923) *A Special Report on the Mortality from Influenza in New York State During the Epidemic of 1918–19*. (NY State Dept Health, Albany).
9. Wallinga J, Teunis P (2004) Different epidemic curves for severe acute respiratory syndrome reveal similar impacts of control measures. *Am J Epidemiol* 160:509–516.
10. Wallinga J, Lipsitch M (2007) How generation intervals shape the relationship between growth rates and reproductive numbers. *Proc Biol Sci* 274:599–604.
11. Fraser C (2007) Estimating individual and household reproduction numbers in an emerging epidemic. *PLoS ONE* 2:e758.
12. Anonymous (Sept 27, 1918) Medical men are told of Influenza's spread. *Philadelphia Record*.
13. Barry JM (2004) *The Great Influenza: The Epic Story of the Deadliest Plague in History*. (Viking, New York).
14. Anonymous (Oct 2, 1918) Spread of Influenza grows serious in city. *Philadelphia Record*.
15. Crosby AW (2003) *America's Forgotten Pandemic*: *The Influenza of 1918*. (Cambridge Univ Press, New York).
16. Frost WH (1920) Statistics of influenza morbidity. With special reference to certain factors in case incidence and case-fatality. *Public Health Rep* 35:584–597.
17. Britten RH (1932) The incidence of epidemic influenza, 1918–19. *Public Health Rep* 47:303–339.
18. Bootsma M, Ferguson N (2007) The effect of public health measures on the 1918 influenza pandemic in U.S. cities. *Proc Natl Acad Sci USA* 104:7588–7593.
19. Hatchett RJ, Mecher CE, Lipsitch M (2007) Public health interventions and epidemic intensity during the 1918 influenza pandemic. *Proc of Nat Acad Sci USA* 104:7582–7587.
20. Clarke SK, Heath RB, Sutton RN, Stuart–Harris CH (1958) Serolgical studies with the Asian strain of influenza A. *Lancet* 1:814–818.
21. Davis LE, Caldwell GG, Lynch RE, Bailey RE, Chin TD (1970) Hong Kong influenza: The epidemiologic features of a high school family study analyzed and compared with a similar study during the 1957 Asian influenza epidemic. *Am J Epidemiol*, 92:240–247.
22. Carrat F, et al. (2008) Time lines of infection and disease in human influenza: A review of volunteer challenge studies. *Am J Epidem* 167:775–785.
23. White LF, Pagano M (2008) Transmissibility of the influenza virus in the 1918 pandemic. *PLoS ONE* 3:e1498.
24. Svensson A (2007) A note on generation times in epidemic models. *Math BioSci*, 208:390–394.
25. Ferguson NM, et al. (2005) Strategies for containing an emerging influenza pandemic in Southeast Asia. *Nature* 437:209–214.
26. Dempster AP, Laird NM, Rubin DB (1997) Maximum likelihood from incomplete data via the EM algorithm. *J R Stat Soc Ser B* 39:1–38.
27. Kenah E, Lipsitch M, Robins JM (2008) Generation interval contraction and epidemic data analysis. *Math BioSci* 213:71–79.
28. Lipsitch M, et al. (2003) Transmission dynamics and control of severe acute respiratory syndrome. *Science* 300:1966–1970.
29. Shepp LA, Vardi Y (1982) Maximum likelihood reconstruction for emission tomography. *IEEE Trans Med Imaging* 113:113–122.

SUPPORTING INFORMATION FOR: DECONVOLUTION AND ESTIMATION FOR EPIDEMIC DATA..

E. Goldstein[a1], J. Dushoff[b,c], J. Ma [d], J.B. Plotkin[e], D.J.D. Earn[d,c], M. Lipsitch[a]

(a) Department of Epidemiology, Harvard School of Public Health, Boston MA, USA (b) Department of Biology, McMaster University, Hamilton, Ontario, Canada (c) M. G. deGroote Institute for Infectious Disease Research, Hamilton, Ontario, Canada (d) Department of Mathematics and Statistics, McMaster University, Hamilton, Ontario, Canada (e) Department of Biology, University of Pennsylvania, Philadelphia PA, USA

1. Richardson-Lucy-type deconvolution

The deconvolution problem (described in detail in (6), with full mathematical derivation of its properties) involves k distinct sources numbered $t_1, ..., t_2$ ($k = t_2 - t_1 + 1$). At each source there is a random, Poisson number of emissions, with unknown Poisson parameters $\lambda_{t_1}, \ldots, \lambda_{t_2}$. There are m detectors numbered $1, \ldots, m$. Each emission from source j can be observed by at most one detector i, and the probability for each such observation is p_{ij}. We assume that for each j, $q_j = \sum_i p_{ij}$ is positive (at least some fraction of emissions from each source is observed), but we drop the assumption, commonly used in the optics literature, that $q_j = 1$ (some of the data might be lost). Given the observations $D_1, \ldots, D_m$ and the known transition probabilities p_{ij}, the deconvolution problem asks for the Poisson parameters λ_j for which the observations have the highest probability (maximum likelihood). The Richardson-Lucy iterative algorithm, which is an EM algorithm (3) solves the above problem. The original Richardson-Lucy algorithm assumes that $q_j = 1$. We can, however, reduce our problem to the Richardson-Lucy scenario, by counting only emissions at each source which are observed. Those are Poisson variables with parameters $\hat{\lambda}_j = q_j \lambda_j$, and the observation probabilities are $\hat{p}_{ij} = p_{ij}/q_j$.

In the epidemiological context, the death curve $D_1, \ldots, D_m$ giving the number of deaths occuring each day represents the detectors. To understand the sources, let $I_{t_1}, \ldots, I_{t_2}$ be the number of people infected on each day. Here $(t_1, \ldots, t_2)$ is a time period, which in general will overlap with the period $(1, \ldots, m)$ for which the daily counts for the number of deaths are available. Since over 95% of deaths for the 1918 influenza happened within 3 weeks of infection, we want to estimate incidence from day $t_1 = -20$ (3 weeks prior to the available death data); we also take $t_2 = m-2$ as $d_0 = d_1 = 0$ for our time-to-death distribution. Thus the number of unknown parameters is $m + 19$, exceeding the number m of observations. Let p be the case fatality ratio, i.e. the probability that an infected person will die from influenza or a secondary pneumonia. It is estimated that p is between $2 - 3\%$ (7; 5; 1). The number of deaths among people infected on day j is thus a binomial variable $B(I_j, p)$. Since I_j is large and p is small, $B(I_j, p)$ is well approximated by

[1]Author for correspondence (egoldste@hsph.harvard.edu)

a Poisson variable with (an unknown) mean $\lambda_j = p \cdot I_j$ - these are the "emissions" from source j. To describe the transition probabilities, let $(d_1, \ldots, d_{31})$ be the time-to-death distribution for the 1918 influenza. Here d_k represents the probability that an infected person who will eventually die, will die on day k after infection. Thus the transition probability p_{ij} (the probability that a person, infected on day j who will eventually die, will die on day i) is

$$p_{ij} = d_{i-j} \; for \; i > j$$

Thus $q_j = 1$, unless $j > m - 31$ (those are days close to the end of the observation period for the death curve), in which case $q_j = \sum_{k=1}^{m-j} d_k$; or $j < 1$ (those are days before the beginning of the observation period for the death curve), in which case $q_j = \sum_{k=-j+1}^{31} d_k$.

Returning to the deconvolution problem, we start with some initial guess $\hat{\lambda}_{t_1}^0, \ldots, \hat{\lambda}_{t_2}^0$ for the parameters $\hat{\lambda}_{t_1}, \ldots, \hat{\lambda}_{t_2}$. For the 1918 flu, we pick the initial parameters to be the death curve shifted back by 9 days, as day 9 since infection is most likely for dying. We then apply the EM algorithm to generate the successive iterations $\hat{\lambda}^n$. The unobserved random variables at each step of the expectation maximization are the X_{ij} - the number of deaths on day i resulting from incidence on day j. These are independent (conditional on the incidence curve) and Poisson distributed, with means $\hat{p}_{ij}\hat{\lambda}_j^n$. The exact recursive formulas are as follows: Let $\hat{\lambda}_{t_1}^n, \ldots, \hat{\lambda}_{t_2}^n$ be the n^{th} iteration for the Poisson parameters. Let $D_i^n = \sum_j \hat{p}_{ij}\hat{\lambda}_j^n$ be the expected number of deaths to occur on day i. Then

$$\hat{\lambda}_j^{n+1} = \hat{\lambda}_j^n \cdot \sum_i \frac{\hat{p}_{ij} D_i}{D_i^n}$$

If we look at $\lambda_j^n = \hat{\lambda}_j^n / q_j$ (which are the Poisson parameters at the n^{th} iteration for all deaths, not just the observed ones, resulting from incidence on day j), those obey the following recursive equations:

$$\lambda_j^{n+1} = \frac{\lambda_j^n}{q_j} \cdot \sum_i \frac{p_{ij} D_i}{D_i^n} \tag{1}$$

We note that the next iteration λ^{n+1} represents the expected numbers of deaths resulting from incidence on each day, conditional on the previous Poisson parameters λ^n and the observed death curve. Also for each successive set of parameters, the observations have higher probability than for the previous parameters. Finally it can be shown, (6), that the iteration converges to a global maximum likelihood solution λ^{ml}. The answer λ^{ml} is characterized by the fact that conditional on the Poisson parameters λ^{ml} and the observations, the expected number of deaths resulting from incidence on day j equals λ_j^{ml}.

We now address some practical issues related to deconvolution, in the context of incidence and deaths. If $\lambda_{t_1}, \ldots, \lambda_{t_2}$ are the true values of the Poisson parameters from which the observables $D_1, \ldots, D_m$ were generated, then D_i does not necessarily equal the expected value $D_i^* = \sum_j p_{ij}\lambda_j$ of the number of deaths on day i. This departure from the expected value is called Type II noise (with Type I noise being the imperfections of the system and its departure from the model). As a result, the maximum likelihood solution described above will approximate the observations closer than the actual parameters λ_j, and the noise will effectively become part

of the answer. It turns out that it is better to stop the Richardson Lucy process after several iterations when the approximation of observations by expectations is reasonable but not too accurate.

To describe the approximation error, let $\lambda^n_{t_1}, \ldots, \lambda^n_{t_2}$ be the result of the n^{th} Richardson Lucy iteration, and let $D^n_i = \sum_j p_{ij}\lambda^n_j$ be the expected number of deaths on day i, as before, with D_i being the observed value. If λ^n were the true parameters, D_i would be Poisson distributed with mean D^n_i; thus the expectation $E(\frac{(D^n_i - D_i)^2}{D^n_i})$ would be 1. This suggests the approach of iterating until the normalized χ^2 statistic

$$\chi^2 = \frac{1}{N_0}\sum_i \frac{(D^n_i - D_i)^2}{D^n_i} \tag{2}$$

descends below 1 for the first time. Here the sum is taken over N_0 observations (death counts). We can use N_0 to be the whole death curve, or just the part with the bulk of deaths, from ascent to descent; the difference for our data is minor.

One may wonder how close is the deconvolved curve to the (unknown) incidence curve. We address this issue in section 4.

2. Time to Death distribution

A collection of distributions for the time from symptom onset to death in various data sets is given in (2) - we refer the reader to that paper for a discussion and comparison. Some of the distributions come from the military, some are civilian, and the latter are generally somewhat shorter. In the main body of the paper we use the distribution of time from symptom onset to death from 599 patients in Cook County Hospital, Chicago. This distribution has a bit of a spike on day 7, suggesting that some smoothing is needed. We used a three day smoothing of the following nature: if $(h_1, \ldots, h_{28})$ is the Cook County distribution, then the distribution we used for the time from symptom onset to death is $(l_1, \ldots, l_{28})$, where

$$l_i = (k_i + \frac{k_{i-1} + k_{i+1}}{2})/2$$

We then convolved $(l_1, \ldots, l_{28})$ with the latent period distribution from (4) to obtain the time to death distribution, used in the main body of the paper. It is plotted in Figure 1. Note that its peak is centered around day 9.

An alternative distribution for time from symptom onset to death is given by the data from 234 autopsy reports from US Army Camp Pike (2). This distribution is somewhat longer that the civilian one; Figure 2 plots the cumulative distribution functions in both cases.

The main body of the paper uses the Cook County Hospital distribution to estimate the incidence curve in Philadelphia. As a sensitivity analysis, the method was repeated using the Camp Pike distribution. The results are plotted in Figure 3. Note that the exponential growth period for incidence still ends on Sep. 26, while the incidence now peaks on Sep. 30 - Oct. 1.

3. Growth rate reproductive number

In the main body of the text, we estimate the daily reproductive numbers R_t using the deconvolved incidence curve and the infectiousness profile distribution, essentially taken from (4). Let the infectiousness profile distribution be $(w_1, \ldots, w_{10})$

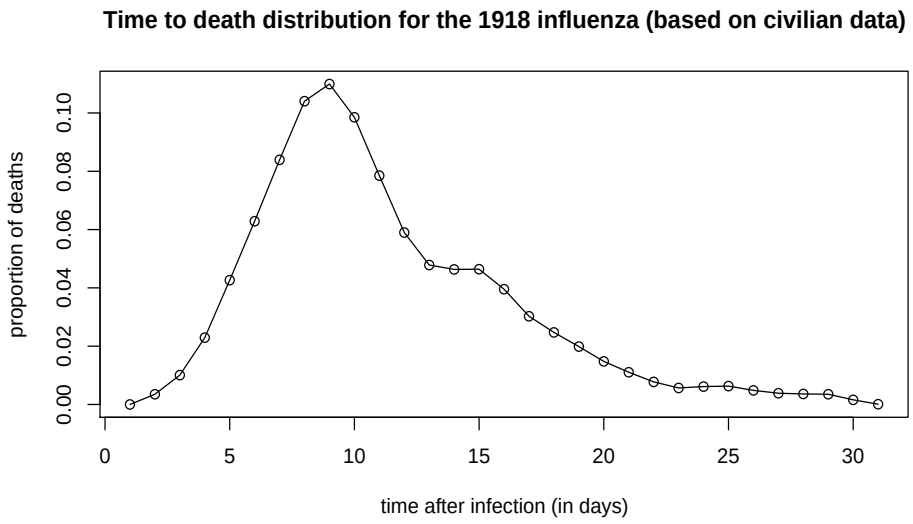

FIGURE 1. Assumed proportions of deaths on each day since infection. Based on the Cook County Hospital data from (2) for time from symptom onset to death, and the latent period distribution from (4).

FIGURE 2. This graph plots the cumulative distribution functions for time from infection to death, based on two data sets for time from symptom onset to death (and the same latent period distribution from (4)). Black (1) is from Cook county hospital, Red (2) - from US Army camp Pike - both taken from (2)

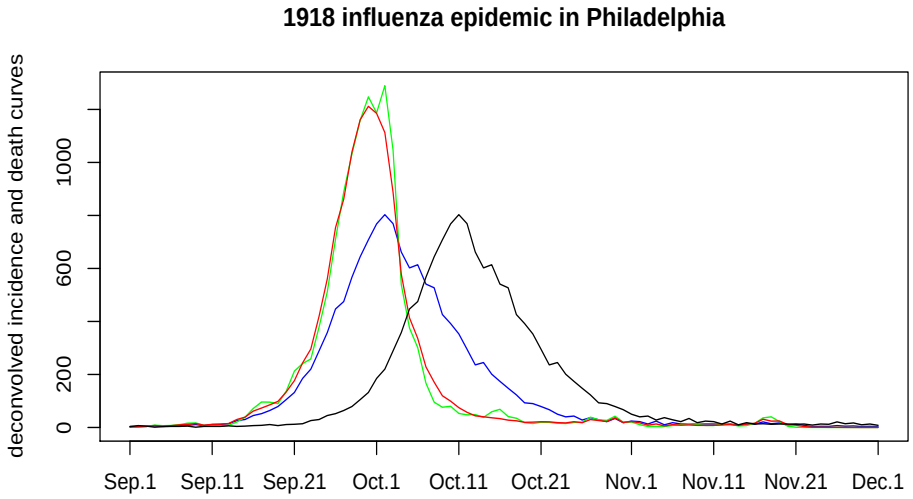

FIGURE 3. This graph plots the flu epidemic in Philadelphia, using the distribution (2) from Figure 2 for time from infection to death. Black is death curve. Blue is the initial condition for RL (death curve, shifted back by 9 days). Red is the assumed answer for incidence, obtained from the first iteration for which the χ^2 value from equation 2 is below 1 (19^{th} iteration). Green are results of RL after 100 iterations.

- it is plotted in Figure 4. Here each number w_i represents the proportion of the cumulative infectiousness which falls between time $(i - 0.5, i + 0.5)$ for an average person. Note that conveniently the latent period in (4) has an offset of 0.5 days.

The estimated reproductive numbers fluctuate in the early part of the epidemic. With this fluctuation of the reproductive numbers, one may wonder what is the best method to estimate the reproductive number R_0 for the early stages of the actual epidemic curve in Philadelphia. The most stable method we have found uses the average growth rate over some reasonably large interval where the growth is approximately exponential. Recall that if the epidemic is growing exponentially with a daily rate r, and if $(w_1, \ldots, w_{10})$ is the infectiousness profile distribution, then the reproductive number R during that period can be found from the equation (8)

$$\frac{1}{R} = \sum_{i=1}^{10} w_i e^{-ir} \tag{3}$$

To assess the exponential growth period, we first plot the natural logarithm of the deconvolved incidence between Sep. 10 and Oct. 4. in Figure 5.

We see that the growth in Figure 5 slows down after Sep. 26; also the incidence is low and fluctuating before Sep. 14. It is reasonable to assume that the actual incidence curve grew exponentially between Sep. 14 and 26, with an unknown

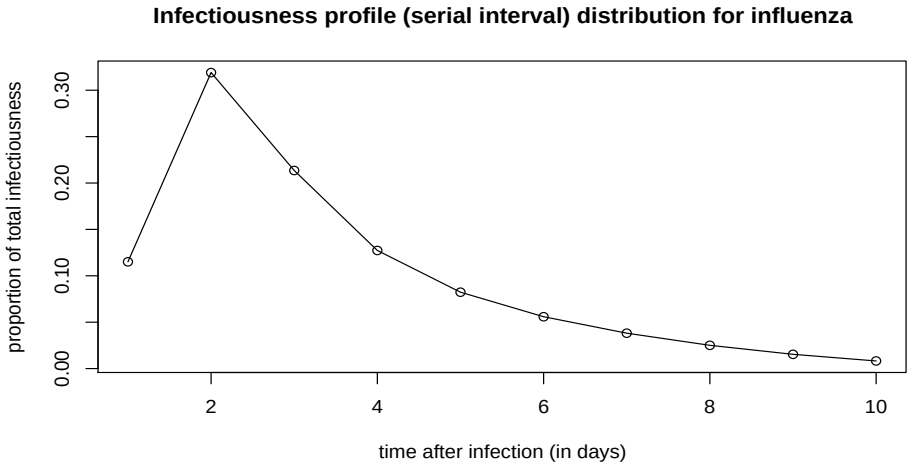

FIGURE 4. Infectiousness profile distribution for influenza, essentially taken from (4). Each number w_i represents the proportion of the cumulative infectiousness which falls between time $(i - 0.5, i + 0.5)$ for an average person. Note that conveniently the latent period has an offset of 0.5 days.

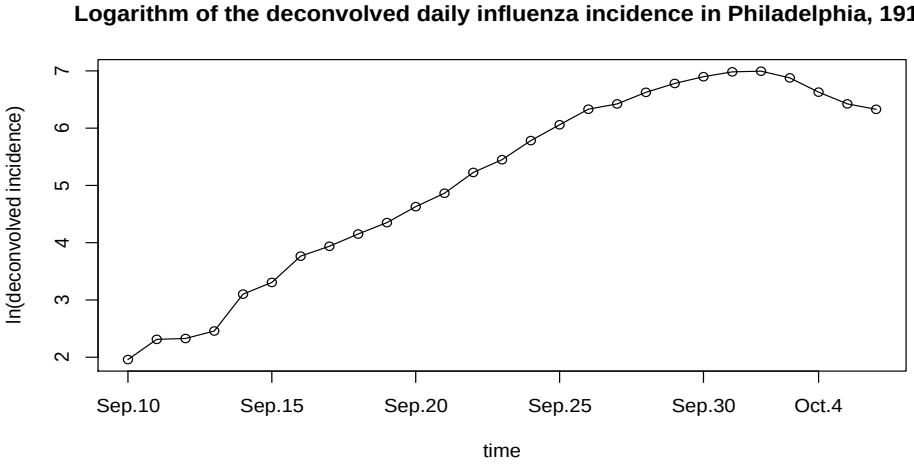

FIGURE 5. Logarithm of the deconvolved Philadelphia incidence, Sep. 10- Oct. 4

growth rate. We can try to infer that growth rate from our deconvolved data; such an inference process might have a bias. To address this, first note that the average growth rate during Sep. 14-26 is $r = (\ln(I(\text{Sep.26})) - \ln(I(\text{Sep.14})))/12 = 0.2690697$. The resulting reproductive number from equation 3 is $R = 2.19$. The bias in such an estimate is assessed by bootstrapping in section 4. Over the period of

Sep. 14-26, the estimated bias is about 0.05, and the standard error of the estimate is 0.13. Thus we estimate $R_0 = 2.14$. Taking shorter periods for computing the growth rate increases the bias - see Table 1.

4. Deconvolved Incidence vs. Actual Incidence

The goal of this section is to use simulations to compare deconvolved incidence curves to the original one. In the process, we also assess the bias that the growth rate reproductive number estimation method from equation 3 gives. We will work this out in three sets of examples. The first involves a civilian time to death distribution from Figure 1; the second involves a military one from Figure 2; the third one allows for some Gaussian noise for the Poisson binning.

In all cases the strategy is as follows: first we generate a "synthetic" incidence curve with a constant initial growth rate to approximate the deconvolved Philadelphia incidence. Next, from this incidence curve and time to death distribution, we generate 500 death curves via Poisson binning (and adding Gaussian noise in the last example). Each of these curves is deconvolved using the initialization procedure and the stopping criterion for iterations which were used for the 1918 data. Those curves are compared to the original one, and their growth rate reproductive numbers are investigated.

4.1. **Civilian time to death distribution.** We generate a "synthetic" incidence curve with a constant initial growth rate to approximate the deconvolved Philadelphia incidence from the main body of the paper. The idea is that if we know the infectivity ratio IR_t on day t and incidence up to day $t-1$, we obtain the incidence on day t by

$$I_t = \mathrm{IR}_t \cdot \sum_{i=1}^{10} I_{t-i} \cdot w_i$$

We prescribe the initial incidence up to day 22, growing exponentially between days 8-22 with the rate compatible with the reproductive number of 2.15, the infectiousness profile distribution and equation 3. We keep the infectivity ratio (and the growth rate) constant at 2.15 up to day 48. We then vary it linearly during several periods to mimic the behaviour of the Philadelphia incidence. The synthetic incidence vs. the deconvolved Philadelphia incidence are depicted in Figure 6.

Next, from this incidence curve and time to death distribution from Figure 1, we generate 500 death curves via Poisson binning. Each of these curves is deconvolved using the initialization procedure and the stopping criterion from section 1. Since the deconvolved Philadelphia incidence took 6 iterations to have the χ^2 statistic descend below 1, we discard those incidence curves which took more than 25 RL iterations - those are 37 curves out of 500. To illustrate the general comparison between deconvolved incidence and the original one, we plot two sets of 5 randomly chosen deconvolved incidence curves against the original one in Figure 7. The plots show that it is sensible to compare their growth rates to the growth rate of the original one during the exponential growth period.

For a pair of days $t_1 < t_2$ (with 1=Sep. 1) and an incidence curve, we compute the average growth rate during that period as

$$r(t_1, t_2) = (\ln(I(t_2)) - \ln(I(t_1)))/(t_2 - t_1) \tag{4}$$

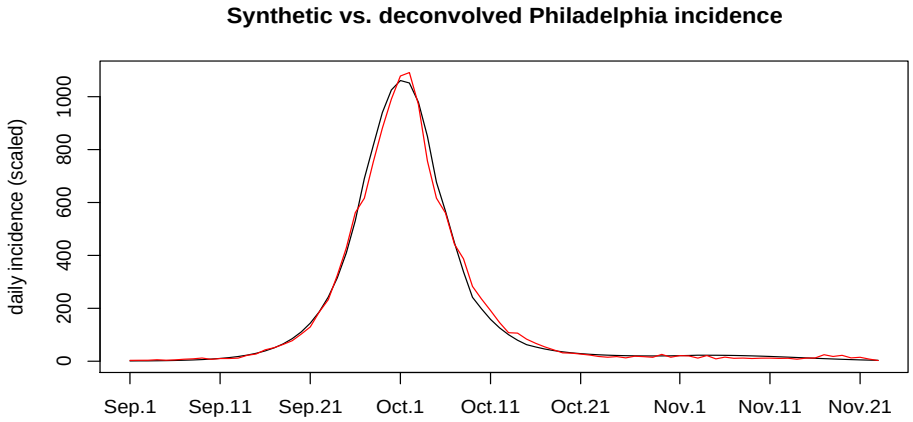

FIGURE 6. "Synthetic" incidence (black) vs. deconvolved Philadelphia incidence from the main body of the paper (red).

Day	Sep.22	Sep.23	Sep.24	Sep.25	Sep.26
Sep.12	b=0.0604 sd=0.2085	b=0.0656 sd=0.1868	b=0.0710 sd=0.1709	b=0.0683 sd=0.1578	b=0.0551 sd=0.1432
Sep.13	b=0.0539 sd=0.1941	b=0.0604 sd=0.1733	b=0.0669 sd=0.1596	b=0.0643 sd=0.1440	b=0.0505 sd= 0.1325
Sep.14	b=0.0560 sd=0.2036	b=0.0630 sd= 0.1792	b=0.0698 sd=0.1611	b=0.0643 sd=0.1420	b=0.0515 sd=0.1300
Sep.15	b=0.0679 sd=0.2213	b=0.0741 sd=0.1891	b=0.0802 sd=0.1661	b=0.0757 sd=0.1485	b=0.0583 sd=0.1320
Sep.16	b=0.0765 sd=0.2199	b=0.0823 sd=0.1814	b=0.0886 sd=0.1620	b=0.0825 sd=0.1389	b=0.0627 sd=0.1219
Sep.17	b=0.0997 sd=0.2401	b=0.1024 sd=0.1884	b=0.1063 sd=0.1609	b=0.0974 sd=0.1379	b=0.0737 sd= 0.1206

TABLE 1. Bias and standard deviation for the reproductive number estimates from section 4.1 for pairs of days, via equations 4 and 3.

The growth rate reproductive number $R(t_1, t_2)$ is obtained from $r(t_1, t_2)$ using equation 3. For $12 \leq t_1 \leq 17$, and $22 \leq t_2 \leq 26$, we tabulate (Table 1) the bias between the mean of those numbers among the 463 deconvolved curves and 2.15, which is the growth rate reproductive number during that period for the synthetic curve from Figure 6. We also include the standard deviation of the estimate.

We note that the choice $(t_1, t_2) = (14, 26)$ (used in section 3) corresponds both to a low bias and a low standard deviation.

4.2. **Military time to death distribution.** In this section, we use time to death distribution (2) from Figure 2. We follow the same protocol as in section 4.1. We

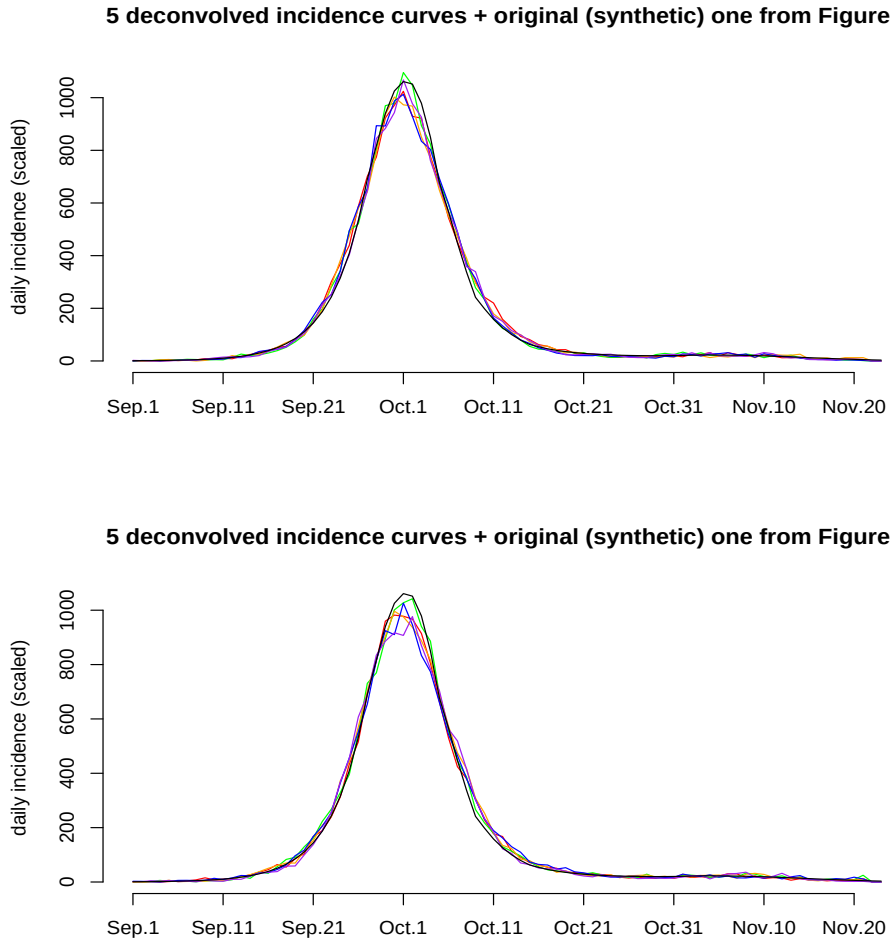

FIGURE 7. Two samples of five deconvolved incidence curves + the original, "synthetic" one from Figure 6 (black).

generate a synthetic incidence curve to fit the deconvolved incidence from Figure 3. The two curves are plotted in Figure 8.

Next, as in section 4.1, we generate 500 "deconvolved" incidence curves, which are results of the Richardson-Lucy deconvolution procedure applied to 500 death curves obtained via Poisson binning of the synthetic incidence curve with respect to the military time-to-death distribution . 52 curves which took more than 30 RL iterations are discarded. We plot two sets of 5 randomly chosen deconvolved incidence curves against the original one in Figure 9.

For days $12 \leq t_1 \leq 17$, and $22 \leq t_2 \leq 26$, we tabulate (Table 2) the bias between the mean of the growth rate reproductive numbers $R(t_1, t_2)$ among the 448 deconvolved curves and 2.16, which is the growth rate reproductive number

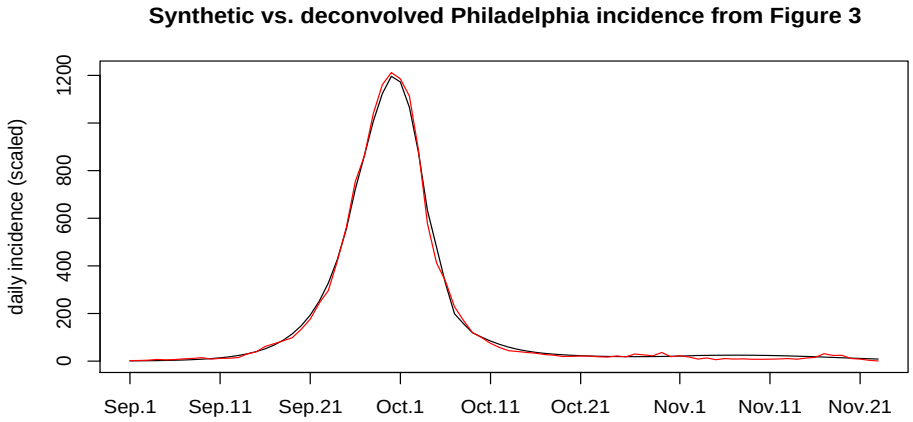

FIGURE 8. "Synthetic" incidence (black) vs. deconvolved Philadelphia incidence from Figure 3 (red).

Day	Sep.22	Sep.23	Sep.24	Sep.25	Sep.26
Sep.12	b=0.0742 sd=0.2221	b=0.0846 sd= 0.2004	b=.0837 sd=0.1808	b=0.0722 sd=0.1638	b=0.0452 sd=0.1518
Sep.13	b=0.0888 sd= 0.2077	b=0.0989 sd=0.1843	b=0.0967 sd=0.1651	b=0.0832 sd=0.1483	b=0.0532 sd=0.1360
Sep.14	b=0.0866 sd= 0.2084	b=0.0979 sd=0.1813	b=0.0956 sd=0.1604	b=0.0809 sd=0.1418	b=0.0486 sd=0.1249
Sep.15	b=0.1087 sd=0.2318	b=0.1187 sd=0.2002	b=0.1135 sd=0.1698	b=0.0954 sd=0.1474	b=0.0587 sd=0.1290
Sep.16	b=0.1295 sd=0.2285	b=0.1388 sd=0.1958	b=0.1301 sd= 0.1655	b=0.1080 sd=0.1384	b=0.0663 sd= 0.1218
Sep.17	b=0.1657 sd= 0.2614	b=0.1695 sd= 0.2167	b=0.1559 sd=0.1847	b=0.1275 sd= 0.1509	b=0.0786 sd= 0.1280

TABLE 2. Bias and standard deviation for the reproductive number estimates from section 4.2 for pairs of days, via equations 4 and 3.

during that period for the synthetic curve. We also include the standard deviation of the estimate.

As in section 4.1, we note that the choice $(t_1, t_2) = (14, 26)$ corresponds both to a low bias and a low standard deviation.

4.3. **Adding Gaussian noise.** In this section we follow a similar protocol as in the two previous sections, expect for the following modification: while simulating death curves from synthetic incidence, we add Gaussian noise after Poisson binning. More precisely, using the synthetic incidence curve from Figure 6 and time to death distribution from Figure 1, we generate preliminary death curves using Poisson

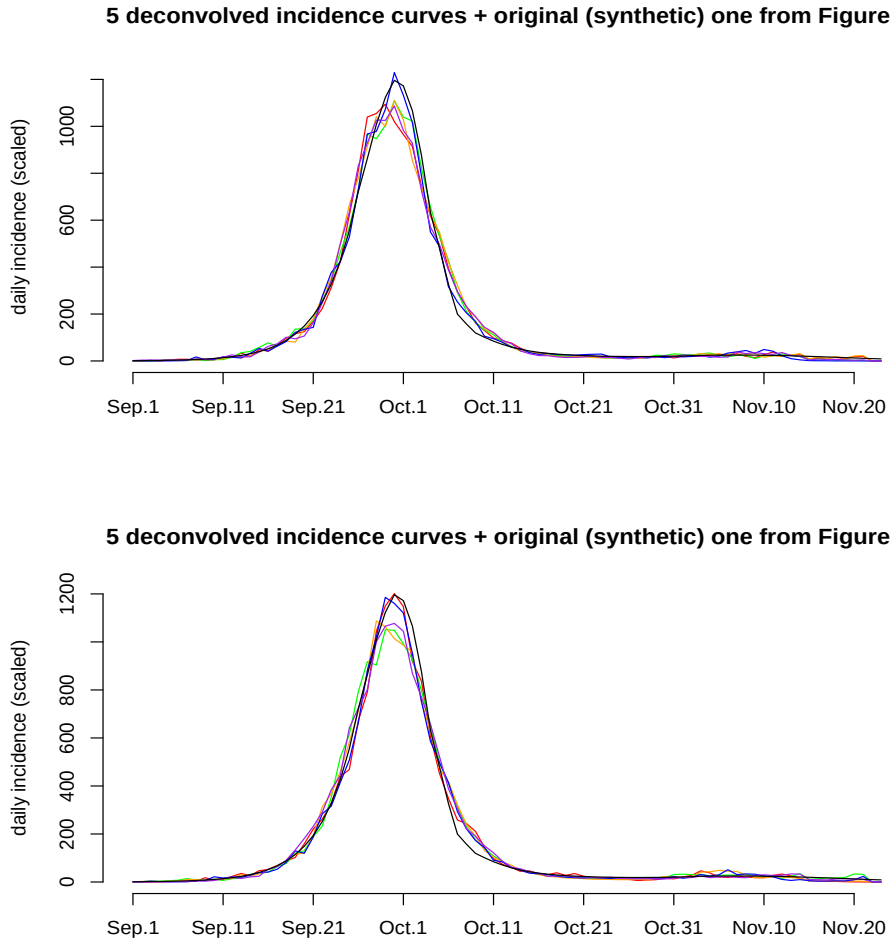

FIGURE 9. Two samples of five deconvolved incidence curves + the original, "synthetic" one from Figure 8 (black).

binning. After that to each count $D(t)$ we add a Gaussian variable $N(0, \sqrt{D(t)}/3)$, restricting the result to the range $(D(t)/2, 3D(t)/2)$. This essentially means that for each death recorded via Poisson binning, there is a probability of 9% that there is an additional ± 1 death.

We generated 500 death curves in that fashion, and deconvolved each, discarding those which took more than 30 iterations for the χ^2 statistic to descend below 1 - these were 79 curves out of 500. As in the previous sections, we record two samples of five deconvolved curves each (Figure 10), as well as the table of biases and standard errors for the growth rate reproductive numbers estimates (Table 3).

Comparing Tables 1 and 3, we note that Gaussian noise generally slightly increases the standard errors and decreases the biases.

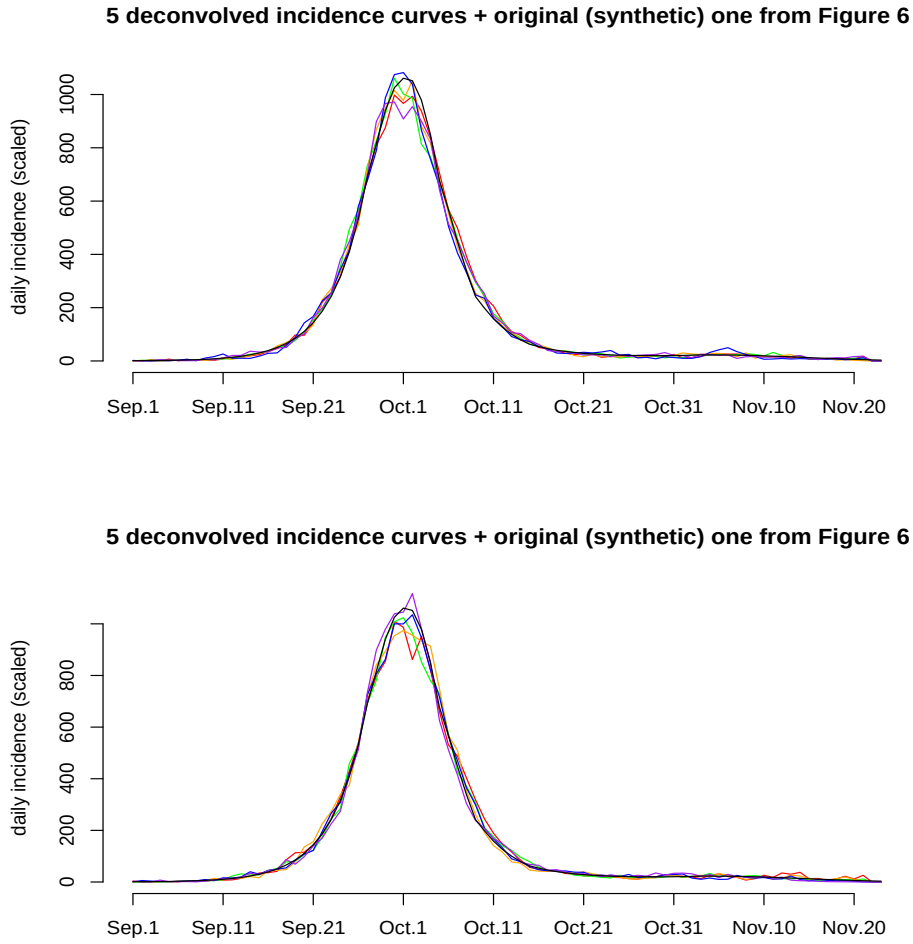

FIGURE 10. Two samples of five deconvolved incidence curves (Gaussian noise added to death curves) + the original, "synthetic" one from Figure 6 (black).

5. Epidemic peak in Philadelphia

In this section we use simulations to examine a key qualitative conclusion we have made in the main body of the text, that the drop in infectivity ratios in Philadelphia between Sep. 26 and Oct. 3 could not be explained by depletion of susceptibles. First we examine the sensitivity of that conclusion with respect to the time-to-death distribution. Then we allow for certain forms of time dependency for the case fatality ratios, reflecting upon potential changes in demographics of the infected as the epidemic progressed. In the simulations we have performed, our conclusion persisted, and the drop in infectivity rations greatly exceeded depletion of susceptibles during that period.

Day	Sep.22	Sep.23	Sep.24	Sep.25	Sep.26
Sep.12	b=0.0473 sd=0.2191	b=0.0541 sd=0.1961	b=0.0582 sd= 0.1774	b=0.0544 sd= 0.1666	b=0.0451 sd=0.1522
Sep.13	b=0.04872 sd=0.2261	b=0.0559 sd=0.1971	b=0.0603 sd=0.1784	b=0.0559 sd=0.1653	b=0.0458 sd=0.1505
Sep.14	b=0.0367 sd=0.2209	b=0.0462 sd= 0.1925	b=0.0520 sd=0.1707	b=0.0479 sd=0.1557	b=0.0377 sd=0.1415
Sep.15	b=0.0564 sd=0.2230	b=0.0647 sd=0.1916	b=0.0690 sd=0.1648	b=0.0627 sd=0.1460	b=0.0503 sd=0.1319
Sep.16	b=0.0840,0.2322) sd=0.2322	b=0.0894 sd=0.1934	b=0.0914 sd=0.1677	b=0.0819 sd= 0.1463	b=0.0661 sd=0.1285
Sep.17	b=0.0928 sd=0.2677	b=0.0976 sd=0.2189	b=0.985 sd=0.1846	b=0.0868 sd= 0.1589	b=0.0685 sd=0.1348

TABLE 3. Bias and standard deviation for the reproductive number estimates from section 4.3 for pairs of days, via equations 4 and 3.

5.1. **Sensitivity with respect to the time-to-death distribution.** In this section we examine the sensitivity of our conclusion about the drop in the infectivity ratios with respect to the time-to-death distribution. First we randomly generate 100 time-to-death distributions as follows:
a) Start with the original time-to-death distribution $d_1, \ldots, d_{31}$ from the main body of the text.
b) Each number d_i is multiplied by $exp(X_i)$, where X_i is a realization of a normally distributed random variable $N(0, 0.5)$ with mean 0 and a standard error 0.5.
c) The numbers $d_i exp(X_i)$ are divided by their sum to form a distribution.

Figure 11 plots two samples of 5 such distributions against the original one.

We deconvolve the Philadelphia death curve using the 100 randomly generated time-to-death distributions above according to the method in the main body of the text. For each such deconvolved incidence curve, we compute the drop in the infectivity ratios between Sep. 26 and Oct. 3, as well as the depletion of susceptibles during that period (both as percentages). We then plot the corresponding 100 pairs of numbers in Figure 12.

We note that our conclusion persists in all the scenarios. In fact, the drop in infectivity ratios surpasses the depletion of susceptibles by a factor of at least 2.68 in all cases.

5.2. **Time-dependence of the case fatality ratios.** In this section we examine the possibility that the case fatality ratio p is time-dependent, thus in fact it equals p_t for day t. This reflects upon potential changes in demographics of the infected as the epidemic progressed. Let I_t be the number of people infected on day t. The number of deaths among people infected on day t is thus a binomial variable $B(I_j, p_t)$. Since I_t is large and p_t is small, $B(I_t, p_t)$ is well approximated by a Poisson variable with (an unknown) mean $\lambda_t = p_t \cdot I_t$. Thus the deconvolution problem in fact seeks an estimate of the numbers (λ_t).

We note that during the exponential growth period of the epidemic with no saturation of susceptibles, different age strata are represented by more-or-less fixed

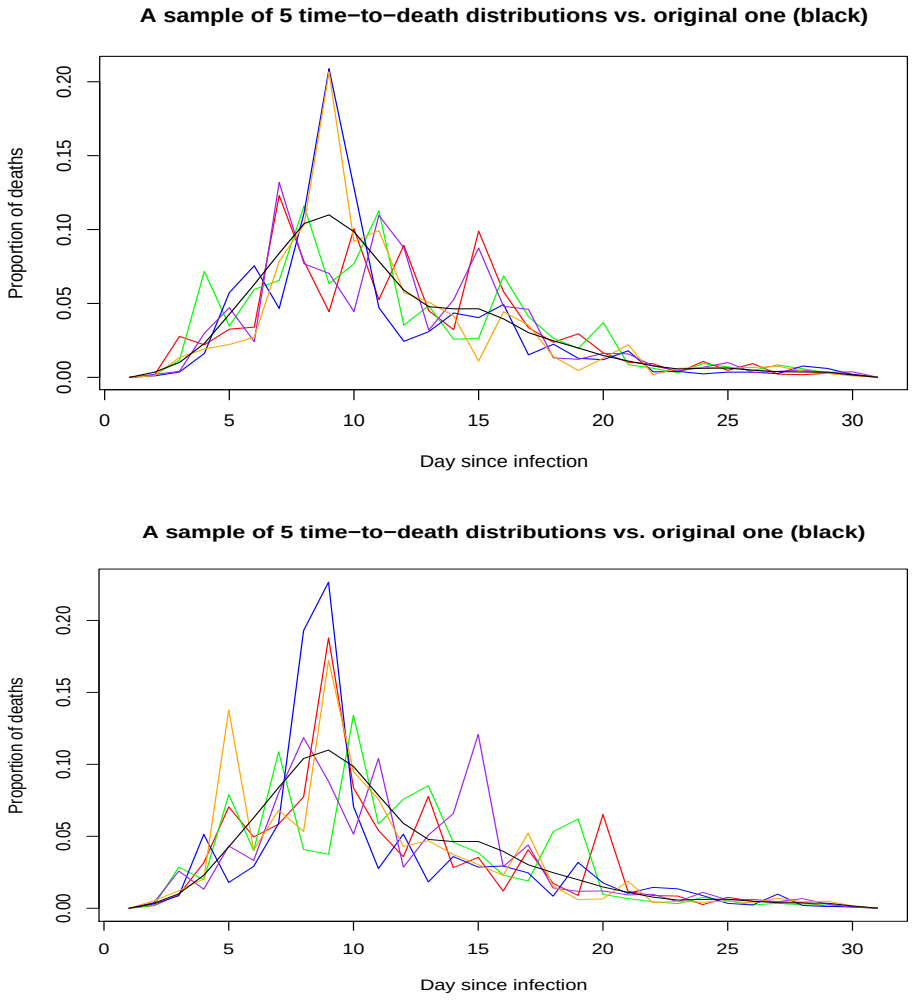

FIGURE 11. Two samples of five randomly generated time-to-death distributions vs. the original one (black).

proportions among the infected, thus p_t changes little. That change starts to occur later, with sizeable depletion of susceptibles.

Recall that the infectivity ratio on day t equals

$$\mathrm{IR}_t = \frac{I_t}{\sum_{s<t} I_s w_{t-s}}$$

Here w_i is the serial interval distribution. Since $(I_t p_t)$ are the deconvolved parameters, we estimate the infectivity ratios as

$$IR_t^{est} = \frac{I_t p_t}{\sum_{s<t} I_s p_s w_{t-s}} \tag{5}$$

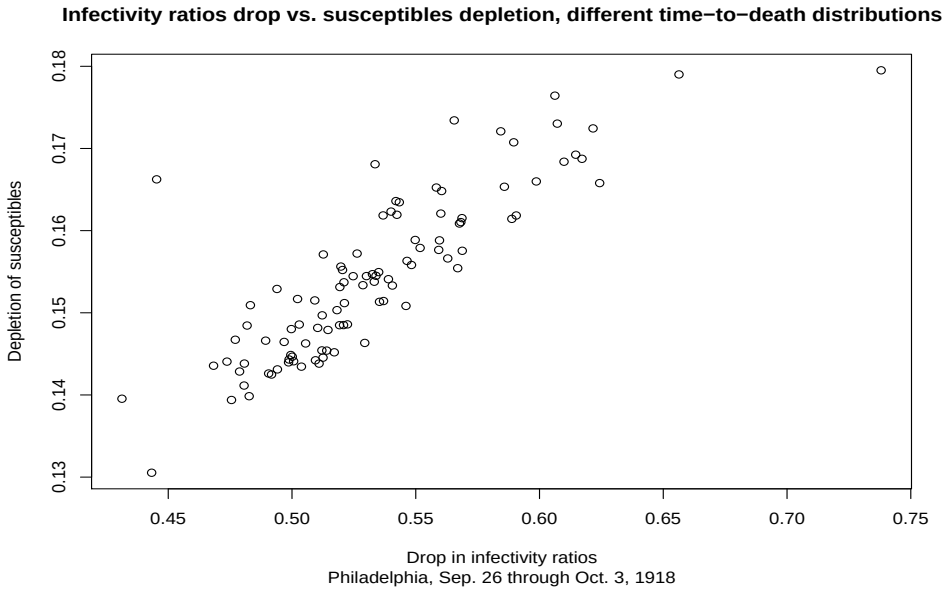

FIGURE 12. Drop in infectivity ratios vs. depletion of susceptibles, Philadelphia, Sep. 26-Oct. 3, 1918. Each pair of point is obtained using a different, randomly-generated time-to-death distribution.

We see that if the case fatality ratios were growing prior to day t, then IR_t^{est} is an overestimate of IR_t; if case fatality ratios were declining prior to day t, when IR_t^{est} is an underestimate of IR_t. When assessing the drop in infectivity ratios between Sep. 26 and Oct.3, we assume the **worst error scenario**, namely that the case fatality ratios were growing prior to Sep. 26 (thus the infectivity ratio on that date is overestimated), and thereafter the case fatality ratios were declining (thus the infectivity ratio on Oct. 3 is underestimated). A phenomenon like that does not appear impossible if we inspect the incidence rates and the case fatality ratios in (5). There, the age group $5-15$ had the highest incidence and the lowest case fatality ratio - thus as that group was getting depleted, case fatality ratios were increasing in time. Later, when the age group $25-35$, which had the highest case fatality ratio, was getting depleted, case fatality ratios p_t were declining in time.

Based on the data in (5) we make an assumption that case fatality ratios were increasing at a rate of 3% a day between Sep. 16 and Sep. 26, and thereafter were decreasing at a rate of 3% a day till at least until Oct. 3 (and probably kept decreasing later as well). Since the serial interval distribution $w_i = 0$ for $i \geq 11$, we see from equation (5) that behavior of the case fatality ratios outside of the specified time interval (Sep. 16 to Oct. 3) does not affect the estimates of infectivity ratios on Sep. 26 and Oct. 3. Relative magnitudes of the case fatality ratios up to Oct. 3 are plotted in Figure 13.

We also note that case fatality ratios from Figure 13 between Sep. 26 and Oct. 3 are greater than their average value over the whole time period, which is assumed to be at least 2%. Thus we maintain our estimate that depletion of susceptibles was at most 16% between Sep. 26 and Oct. 3.

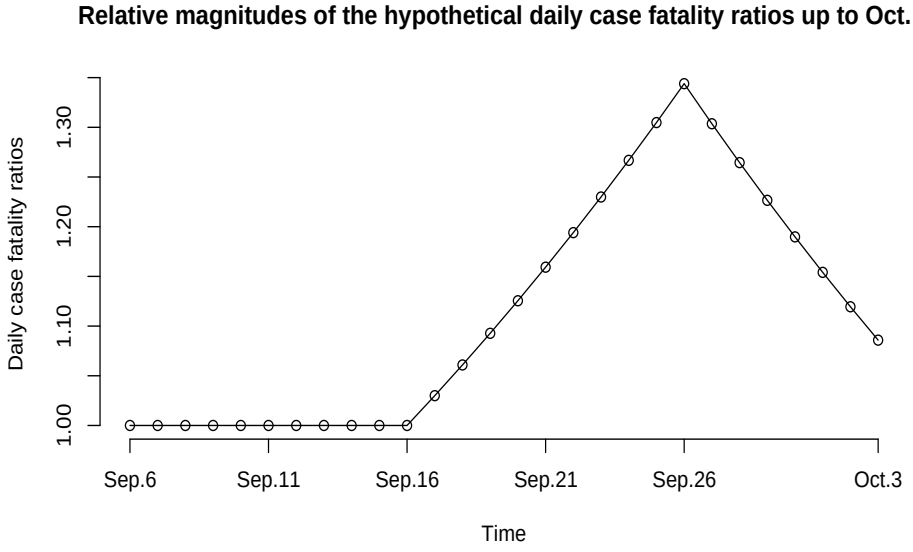

FIGURE 13. Relative magnitudes of hypothetical case fatality ratios up to Oct. 3, 1918 in Philadelphia (relative to the case fatality ratio during the early exponential growth period of the epidemic)

If we assume that the deconvolved Philadelphia incidence curve is the actual incidence curve and the case fatality ratios behave as specified in Figure 13, the actual decline in infectivity ratios between Sep. 26 and Oct. 3 is 0.457 (45.7%), while our estimate with constant case fatality ratios is 0.538. We allow for an additional error resulting from the deconvolution process. This error can be estimated from simulations. While we do not know the original incidence curve, we try to estimate the error using two types of simulations:

Starting from an incidence curve: A starting point in such simulations is a curve $C_t = I_t p_t$, where I_t is an incidence curve and p_t are the case fatality ratios as in Figure 13. A death cruve is generated from C_t via Poisson binning with respect to the time-to-death distribution; this death curve is deconvolved to obtain deconvolved incidence. Since we do not know the original incidence curve, we use the deconvolved incidence curve I_t^{dec} from the main body of the text for C_t.

We have generated 500 "death" curves by Poisson binning of the curve I_t^{dec} with respect to the time-to-death distribution. Each such curve was deconvolved according to the procedures in the main body of the text. "Incidence" curves which took more than 30 iterations to deconvolve were discarded. For the resulting 492 "incidence" curves, drops in the infectivity ratio between Sep. 26 and Oct. 3 were calculated. The maximal drop in infectivity ratios was 0.646. If we take the 95% confidence interval (discarding the 12 largest and the 12 smallest values), the maximal drop among the remaining ones is 0.605. Thus, starting from an incidence curves with a drop of 0.457 in infectivity ratios between Sep. 26 and Oct. 3 and the case fatality ratios p_t as in Figure 13, the 95% confidence bounds for the drop in infectivity ratios from the deconvolved death curve are $(0.437, 0.605)$. Since the drop

in infectivity ratios for I_t^{dec} is 0.538, we estimate with 95% confidence that the drop in infectivity ratios for the original incidence curve is at least $0.457 * 0.538/0.605 = 0.406$

Starting from a death curve: We start from the Philadelphia death curve D_t. We generate 500 "death" curves whose value at time t is the mean of D_t and $\text{Pois}(D_t)$, where $\text{Pois}(D_t)$ is a realization of a Poisson variable with mean D_t (when we considered death curves equaling $\text{Pois}(D_t)$, most of them took over 30 RL iterations to deconvolve). Each such curve is deconvolved; incidence curves which took more than 30 Richardson-Lucy iterations to converge were discarded. The resulting 497 curves were divided by the case fatality ratios p_t from Figure 13. Those are thought of as potential incidence curves in Philadelphia. Drops in infectivity ratios between Sep. 26 and Oct. 3 for these curves were computed. A 95% confidence interval for these drops is $(0.405, 0.5)$.

References

[1] R.H. Britten (1932) *The incidence of epidemic influenza, 1918-19.*, Public Health Rep. 47, pp. 303-39

[2] J.F. Brundage, and D. Shanks (2008) *Deaths from Bacterial Pneumonia during 1918-19 influenza pandemic*, Emerging Infectious Diseases, 14 (8), pp. 1193–1199.

[3] A.P. Dempster, N.M. Laird, and D.B. Rubin (1997) *Maximum likelihood from incomplete data via the EM algorithm*, J. Royal Stat. Soc. Ser. B2, 39 (1), pp. 1–38.

[4] N.M. Ferguson et. al. (2005) *Strategies for containing an emerging influenza pandemic in Southeast Asia*, Nature, 437 (7056), pp. 209–14.

[5] W.H. Frost (1920) *Statistics of influenza morbidity. With special reference to certain factors in case incidence and case-fatality*, Public Health Rep. 35, pp. 584-97

[6] L.A. Shepp, and Y. Vardi (1982) *Maximum Likelihood Reconstruction for Emission Tomography*, IEEE Transactions on Medical Imaging, 113 (1), pp. 113-122

[7] J.K. Taubenberger, and D.M. Morens, *1918 Influenza: the mother of all pandemics*, Emerging Infectious Diseases, 12 (1) (2006), pp. 15–22.

[8] J. Wallinga, and M. Lipsitch (2007) *How generation intervals shape the relationship between growth rates and reproductive numbers*, Proc Biol Sci, 274 (1609), pp. 599–604.